

<https://doi.org/10.1038/s43247-025-03092-5>

# Glacially derived iron is more bioavailable to Antarctic phytoplankton than other sources

Check for updates

Jasmin Stimpfle<sup>1</sup> ✉, Florian Koch<sup>1</sup>, Berenice Ebner<sup>1</sup>, Christian Völkner<sup>1</sup>, Rebecca Zitoun<sup>2,3</sup>, Camila F. Sukekava<sup>3</sup>, Sylvia G. Sander<sup>3,4</sup>, Susann Henkel<sup>1,5</sup>, Randelle M. Bundy<sup>6</sup>, Angel Ruacho<sup>6</sup>, Sabine Kasten<sup>1,5,7</sup> & Scarlett Trimborn<sup>1</sup>

The bioavailability of iron from different sources to phytoplankton, driving substantial carbon dioxide uptake of the large blooms downstream of South Georgia Island, remains unknown. Although geochemical characterization suggests that iron from glacial meltwater and groundwater is bioavailable, phytoplankton iron uptake measurements are lacking. In this study, additional to assessing iron chemical speciation and weathering processes, iron-55 uptake by a natural phytoplankton community was quantified in seawater sampled from low and high chlorophyll waters around South Georgia, to which iron from nearshore sources (glacial meltwater and groundwater) was added. Iron bioavailability depended on the chemistry of the fertilized seawater and the chemical composition of the source itself. Aggregation of dissolved organic matter in high chlorophyll water scavenged dissolved iron, making it unavailable to phytoplankton. In low chlorophyll water, as opposed to iron from groundwater, iron from glacial meltwater was bioavailable to phytoplankton and would increase carbon dioxide fixation by 80–100%.

Primary production in the Southern Ocean (SO) is constrained by the availability of iron (Fe). This results in high concentrations of unutilized macronutrients in seawater<sup>1,2</sup>, making the SO a high-nutrient low-chlorophyll (HNLC) region<sup>3</sup>. Exceptions are observed in the vicinity of islands, where primary production flourishes, sustaining a variety of wildlife<sup>4,5</sup>. This effect is commonly referred to as the Island Mass Effect<sup>5–7</sup>. Physical processes contributing to the Island Mass Effect are well known and promote the entrainment of nutrient and Fe-rich deep waters into the euphotic zone<sup>8</sup>. This process includes, for example, upwelling induced either by topography and shedding of eddies, as well as enhanced vertical mixing due to surface water currents interacting with the island<sup>9,10</sup>. Biogeochemical aspects of the Island Mass Effect, i.e., natural Fe fertilization by lithogenic inputs from the island as well as sedimentary inputs, have been studied before at Kerguelen Island<sup>5,7,11</sup>. Still, little is known about the Fe sources that fuel the high productivity around South Georgia. Primary production around the island has been estimated to be 10 times higher compared to the surrounding Weddell Sea (~200 g C m<sup>-2</sup> yr<sup>-1</sup> vs. ~20 g C m<sup>-2</sup> yr<sup>-1</sup><sup>12</sup>). Observational and modeling studies corroborate that the Fe sources fueling the blooms off South Georgia originate close to the island's shore<sup>13–15</sup>. However, Fe fluxes from different

nearshore sources and their respective bioavailability to phytoplankton remain poorly resolved. A comparison of Fe flux estimates for the Southern Ocean<sup>16</sup> reveals that nearshore sources such as subglacial meltwater (0.005–5.5 mg Fe m<sup>-2</sup> yr<sup>-1</sup>), shelf sediments (0.35–39.5 mg Fe m<sup>-2</sup> yr<sup>-1</sup>) and icebergs (2–20 mg Fe m<sup>-2</sup> yr<sup>-1</sup>) can be significant contributors to the Fe pool in seawater. Atmospheric deposition from dust and aerosols also supplies Fe to the SO<sup>16,17</sup>. At Kerguelen Island, it has been shown that glaciogenic Fe and Fe from the plateau are transported offshore, where seasonal phytoplankton blooms occur<sup>18</sup>. Studies estimating Fe fluxes commonly distinguish certain size classes of dissolved Fe (dFe (<0.2 μm): soluble Fe (<0.02 μm) and colloidal Fe (0.02–0.2 μm)) and assume them to be fully or partially bioavailable<sup>19–22</sup>. Colloids, particles and ligands maintain a large inventory of Fe in the water column, the in situ cycling of which may produce bioavailable species such as the highly bioavailable free inorganic Fe(II). The complex interplay between chemical and physical speciation, such as the complexation with organic ligands and size fractionation, governs Fe bioavailability<sup>23</sup>. Soluble Fe (for example, free inorganic Fe(II)) can be directly taken up by phytoplankton and is therefore most bioavailable<sup>24</sup>. Nevertheless, 30–81% of the dFe pool in the mixed layer is present in the

<sup>1</sup>Alfred Wegener Institute Helmholtz Centre for Polar and Marine Research, Bremerhaven, Germany. <sup>2</sup>Institute for Marine and Antarctic Studies, University of Tasmania, Hobart, TAS, Australia. <sup>3</sup>GEOMAR Helmholtz Centre for Ocean Research Kiel, Kiel, Germany. <sup>4</sup>Faculty of Mathematics and Natural Sciences University of Kiel, Kiel, Germany. <sup>5</sup>MARUM - Center for Marine Environmental Sciences, University of Bremen, Bremen, Germany. <sup>6</sup>University of Washington, Seattle, WA, USA. <sup>7</sup>Faculty of Geosciences University of Bremen, Bremen, Germany. ✉e-mail: [Jasmin.Stimpfle@awi.de](mailto:Jasmin.Stimpfle@awi.de)

form of colloids<sup>24</sup>, and the importance of those chemically dynamic colloids in shaping Fe bioavailability is unclear. For instance, colloids have the potential to serve as a source of Fe for phytoplankton<sup>25,26</sup> but may also lead to the formation of aggregates, scavenging Fe from the euphotic layer<sup>27</sup>. While particulate Fe (pFe >0.2  $\mu\text{m}$ ) is not considered to be bioavailable to phytoplankton, it contributes to the dFe pool by light- or ligand-induced dissolution<sup>28</sup>. Furthermore, after deposition, iron oxides that are part of the particulate iron pool might be subject to anoxic conditions and get reduced, which may result in benthic release of Fe(II) into the water column<sup>29</sup>. Chemical speciation of Fe in seawater adds another level of complexity in determining its bioavailability. Fe-binding ligands are a diverse group of organic molecules that facilitate the dissolution of Fe at higher concentrations than would be possible in its inorganic form, promoting uptake by phytoplankton<sup>30–32</sup>. Ultimately, though, it's the binding strength of the Fe-ligand complex and the physiological traits of the phytoplankton cell, which are thought to determine Fe bioavailability<sup>33,34</sup>. Despite the fact that 99% of dFe in seawater is bound to ligands<sup>35</sup>, governing Fe speciation and bioavailability to a large degree, our understanding of these complexes is limited. Only a few ligands have been thoroughly described, with the majority remaining uncharacterized<sup>35</sup>. For instance, siderophores have been found to form strong Fe complexes, impacting bioavailability to phytoplankton, depending on whether they have siderophore uptake pathways<sup>31,33</sup>. Humic substances and exopolysaccharides, on the other hand, have been shown to

increase Fe bioavailability in the SO<sup>32,36,37</sup>. Previously, dFe and pFe have been quantified in surface waters in the South Georgia region, indicating that shelf sediments, pore waters and glacial meltwaters serve as sources of high Fe concentrations in the surrounding ocean<sup>13</sup>. Likewise, groundwater can substantially contribute to the Fe enrichment of seawater in the SO<sup>38</sup>. Climate change-induced warming will increase melting of glaciers and thawing of permafrost on the island<sup>39</sup> and therefore alter the associated Fe fluxes. However, the bioavailability of Fe originating from these nearshore sources to phytoplankton around South Georgia is still unknown. Accordingly, we sampled different nearshore sources of Fe to assess the bioavailability of Fe to phytoplankton: Groundwater (GW) from a subaerial seepage, featuring reddish precipitates; water from proglacial meltwater (MW) streams, producing turbid plumes in the fjord, as seen on satellite images and water from the estuary (EW), in the mixing zone where the glacial meltwater stream enters the fjord (Figs. 1, 2). Sampling took place in King Haakon Bay (KHB) on the south-western side of the island and in Cumberland Bay (CB) on the north-eastern side (Fig. 1). In the framework of the GEOTRACES process study *Island Impact*<sup>40</sup>, we conducted short-term <sup>55</sup>Fe uptake experiments with a natural, Fe-limited phytoplankton community on board the research vessel *Polarstern*<sup>40</sup>. Water sampled from a low and a high chlorophyll (chl) site was filtered (0.2  $\mu\text{m}$ ; hereafter referred to as low chl water (LCW) and high chl water (HCW, Fig. 1) and enriched with Fe from the above-mentioned nearshore Fe sources. The preconcentrated natural, diatom-

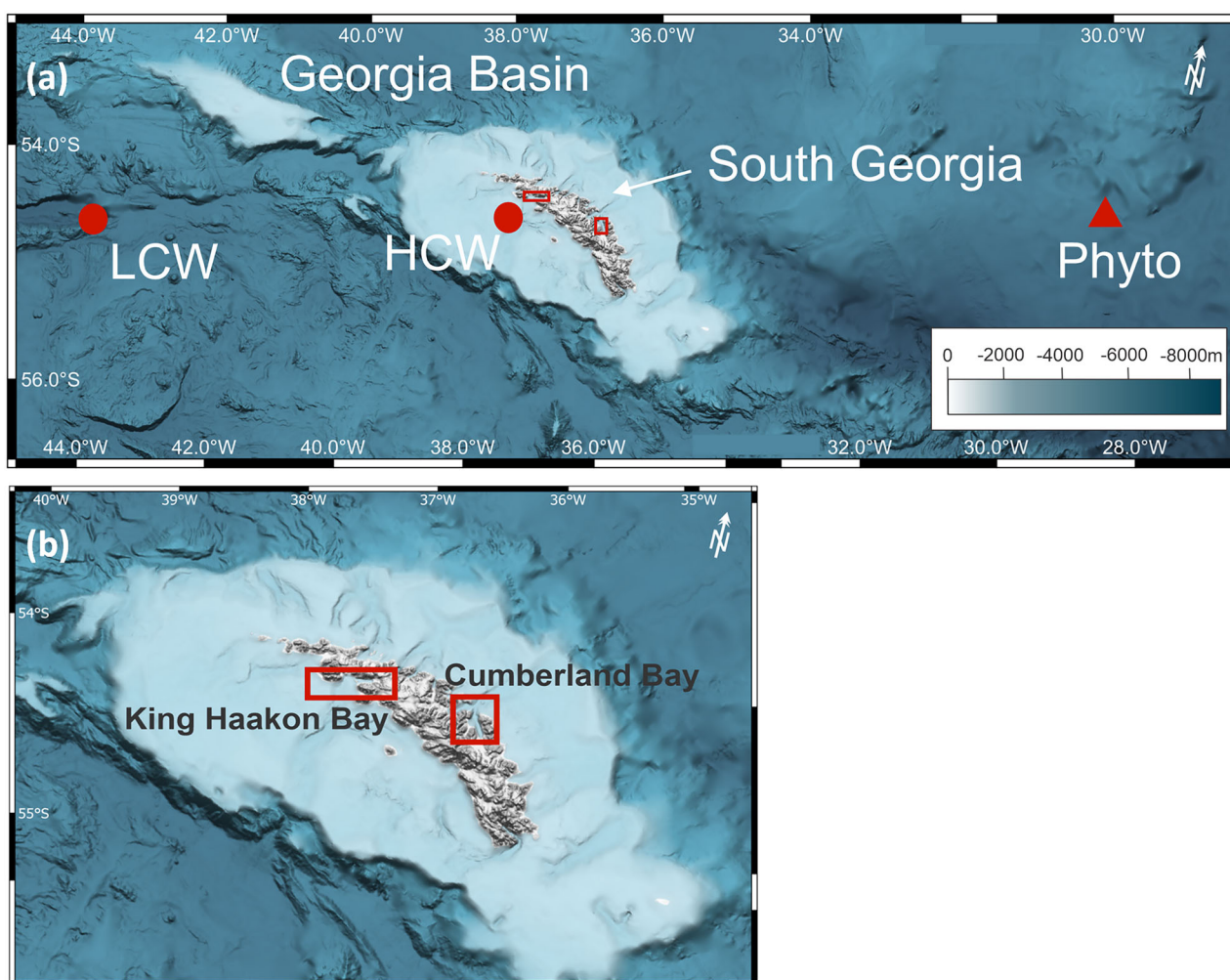
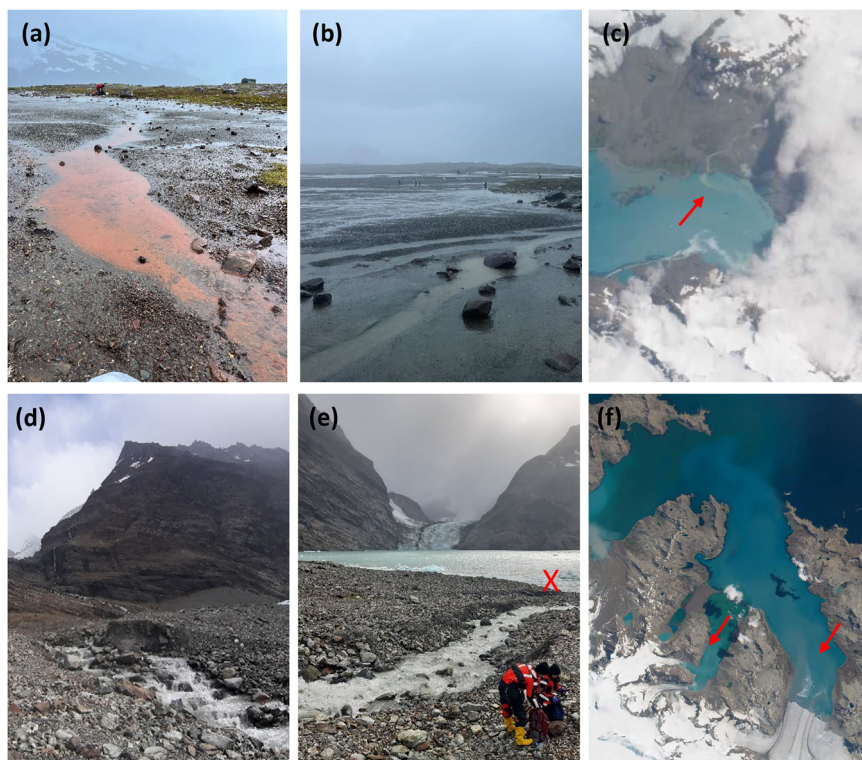


**Fig. 1 | Sampling locations on South Georgia Island.** **a** At two sites, seawater was collected as indicated by the red circles: Low chlorophyll water (LCW) and high chlorophyll water (HCW). To assess the bioavailability of Fe from different sources, a natural Fe-limited phytoplankton community (Phyto, red rectangle) was collected.

**b** The different Fe sources were sampled in King Haakon Bay (south-western side of South Georgia) and Cumberland Bay (north-eastern side) as indicated by the red rectangles. Bathymetry from ref. 104.

**Fig. 2 | Sampling locations of the natural Fe sources on South Georgia Island.** King Haakon Bay: **a** subaerial groundwater seepage, **b** proglacial meltwater stream, **c** satellite picture showing glacial discharge into the fjord. Cumberland Bay: **d** proglacial meltwater stream, **e** estuarine water (sampling location indicated by the red cross), **f** satellite picture showing glacial discharge into the fjord. Photographs by Berenice Ebner (**a**, **b**, **d**) and Katja Laufer-Meiser (**e**, GEOMAR), Satellite images: Sentinel-2 L1C taken 01/2023 and 11/2021.



dominated phytoplankton community (Supplementary Fig. 1) was then added to each treatment and the bioavailability of Fe from each source was determined by measuring  $^{55}\text{Fe}$  uptake in triplicate after 24 h. The uptake experiment also included a treatment with  $\text{FeCl}_3$  and unamended bottles (LCW and HCW without source addition) for comparison (Fig. 3).

## Results and discussion

### Biology and chemistry differ between the two sampling sites

The LCW, sampled at 20 m depth, 450 km off South Georgia (Fig. 1), was characterized by high concentrations of macronutrients (19.02  $\mu\text{M}$  nitrate, 1.30  $\mu\text{M}$  phosphate and 12.56  $\mu\text{M}$  silicate, Supplementary Table 1). The mixed layer depth was 43 m. At this site, low concentrations of chlorophyll *a* (chl *a*, 0.33  $\mu\text{g L}^{-1}$ ) and particulate organic carbon (POC, 0.14  $\text{mg L}^{-1}$ ) were observed, while productivity (27.85  $\text{mg C m}^{-3} \text{d}^{-1}$ ) and photosynthetic efficiency of the in situ phytoplankton community (Fv/Fm, 0.29) were moderate<sup>41</sup>. Likewise, dFe concentration in the LCW was moderate (0.42 nM) and abundance of heterotrophic bacteria was found to be 217,352 cells  $\text{mL}^{-1}$ . The HCW was collected from 20 m depth on the shelf in proximity to the island (<2 km) and this location exhibited similarly high concentrations of macronutrients (16.90  $\mu\text{M}$  nitrate, 1.09  $\mu\text{M}$  phosphate, and 9.54  $\mu\text{M}$  silicate, Supplementary Table 1). However, chl *a* (3.78  $\mu\text{g L}^{-1}$ ), POC (0.37  $\text{mg L}^{-1}$ ), primary production (139  $\text{mg C m}^{-3} \text{d}^{-1}$ ), photosynthetic efficiency (Fv/Fm = 0.43) and bacterial abundance (383,049 cells  $\text{mL}^{-1}$ ) at this location were substantially higher compared to the LCW, indicating the progression of a phytoplankton bloom. Likely due to biological uptake, dFe concentration (0.12 nM) was lower in the HCW than in the LCW<sup>42,43</sup>. DFe at the HCW site was depleted by an intense phytoplankton bloom, which implies that dFe must have been much higher initially. Accordingly, primary production at this site was high, as diatoms still photosynthesize, relying on their intracellular Fe pools<sup>42,43</sup>.

Ligands prevent Fe from precipitation in seawater and thus are essential in governing Fe bioavailability to phytoplankton<sup>33,35</sup>. In most of the open ocean, concentrations of ligands are found to be higher than those of dFe<sup>44</sup>. The total ligand concentration ( $L_T = 0.42 \pm \text{n.d. nM}$ ) of the LCW,

however, exactly matched the dFe concentration, indicating a lack of excess Fe binding ligands ( $L^*$ , the difference between  $L_T$  and dFe) in this batch of seawater (Table 1). Similarly, Boyd and Tagliabue<sup>44</sup> reported that in 12–14% of the oceanwide observations,  $L^*$  was negative- or close to zero. In line with our data, negative  $L^*$  were also found in open ocean waters, for example the south Atlantic<sup>44</sup>. Since the sampling site of the LCW was remote and far away from terrestrial Fe sources, these findings can most probably be attributed to a lack of biological ligand production in this area and/or the photochemical destruction of ligands in surface waters<sup>35,44–46</sup>. In the voltammetric analysis, limited titration resolution prevented reliable determination of the conditional stability constant ( $\log K_{\text{FeL,Fe}'}^{\text{cond}}$ ) with respect to Fe' (free inorganic Fe) for the LCW (Table 1).

In the HCW,  $L_T$  exceeded the dFe concentration, resulting in a plethora of excess ligands ( $L_T = 1.10 \pm 0.48 \text{ nM}$ ;  $L^* = 0.98 \text{ nM}$ , Supplementary Table 2). Using operationally defined ligand classes<sup>35</sup>, the stability constant ( $\log K_{\text{FeL,Fe}'}^{\text{cond}} = 10.49 \pm 0.45$ ) of ligands in the HCW indicate presence of weak binding ligands, influencing Fe bioavailability. As Fe bioavailability is governed by the interplay of  $L_T$  and  $\log K_{\text{FeL,Fe}'}^{\text{cond}}$ , the product of both parameters, termed complexation capacity ( $\alpha = L_T \times 10^{\log K_{\text{FeL,Fe}'}^{\text{cond}}}$ , where  $L_T$  is in  $\text{mol L}^{-1}$ ) will be used henceforth as an explanatory variable<sup>33</sup>. Further, Fe', which is considered to be highly bioavailable, was calculated and equal to  $2.80 \pm 3.12 \text{ pM}$  in the HCW. Altogether, Fe speciation parameters measured in the HCW fall within the range found in other studies of the SO<sup>47–49</sup>.

**Discriminating between chemical and biological Fe removal.** To differentiate between biological and non-biological removal of Fe, bottles of the LCW and HCW (without Fe addition) were split into biotic (addition of pre-concentrated phytoplankton) and abiotic ones (without addition of phytoplankton, Fig. 3). As expected, no Fe uptake occurred in the abiotic LCW due to the absence of phytoplankton cells. Surprisingly,  $^{55}\text{Fe}$  was retained on the filters in the abiotic HCW (Supplementary Table 2). In fact, the amount of  $^{55}\text{Fe}$  in the abiotic HCW was similar to that in the biotic HCW, suggesting an effect driven by chemistry and not by biology. This observation is indicative of the formation of  $^{55}\text{Fe}$ -rich

**Fig. 3 | Experimental setup.** About 0.2- $\mu\text{m}$ -filtered natural Antarctic seawater was collected from a low and high chlorophyll region (LCW and HCW, respectively) around South Georgia Island (Fig. 1). To the LCW and HCW, Fe from the following natural sources was added: groundwater (GW) from a subaerial seepage and proglacial meltwater (MW) from King Haakon Bay and proglacial meltwater (MW) and estuarine water (EW) from Cumberland Bay. The addition of Fe (unfiltered water) from these natural sources was compared to the addition of iron chloride ( $\text{FeCl}_3$ ). A set of LCW and HCW bottles was left unamended (no addition). After allowing each treatment to equilibrate for 24 h, samples for dFe concentrations and Fe speciation were taken. To quantify the Fe bioavailability of each treatment, radioactive Fe ( $^{55}\text{FeCl}_3$ ) was added and left to equilibrate for another 24 h before aliquots of the pre-concentrated Antarctic phytoplankton community (taxonomic composition, Supplementary Fig. 1) were added to the treatments. The LCW and HCW without Fe addition were further split into biotic and abiotic bottles, with only the biotic bottles receiving the phytoplankton concentrate.  $^{55}\text{Fe}$  uptake over 24 h by the respective phytoplankton community was then determined in each treatment.

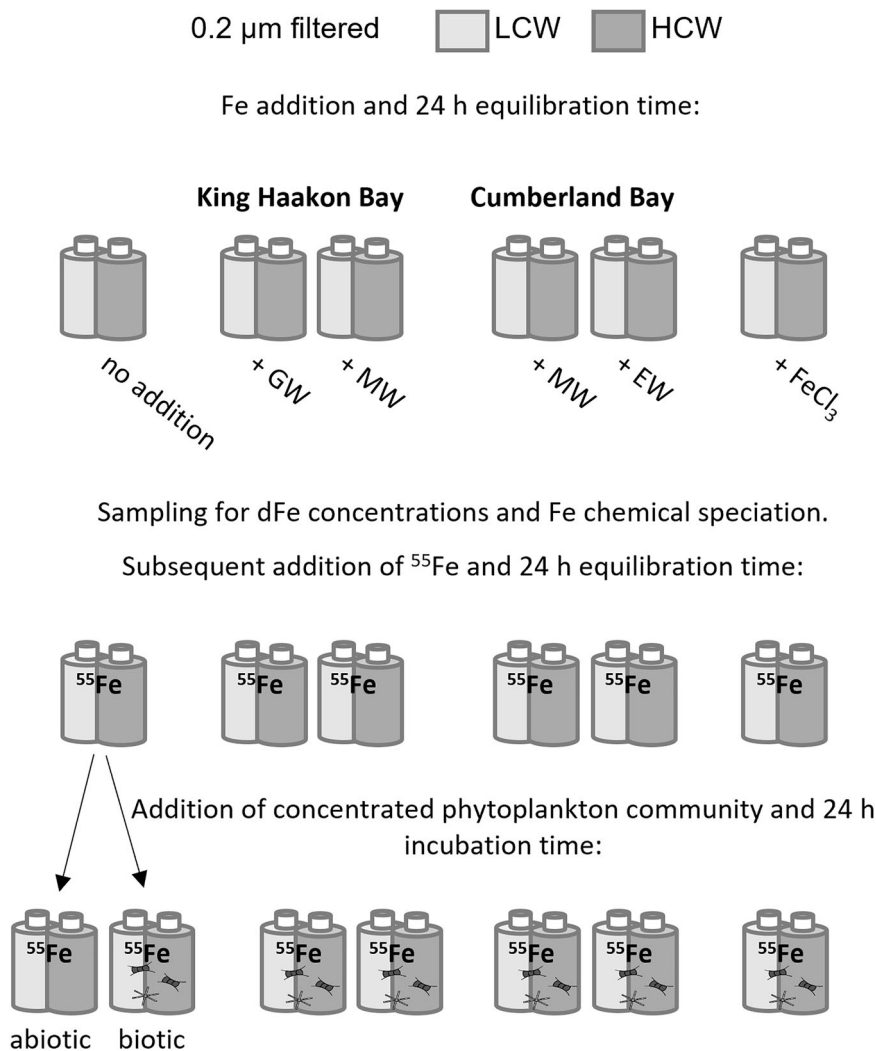


**Table 1 | Fe speciation, dissolved organic matter (DOC) and primary production (PP) in the LCW**

	dFe (nM)	$L_T$ (nM)	$L^*$ (nM)	$\log K_{\text{FeL,Fe}}^{\text{cond}}$	$\alpha$	$\text{Fe}'$ (pM)	DOC ( $\mu\text{mol L}^{-1}$ )	PP ( $\mu\text{g C L}^{-1} \text{d}^{-1}$ )
LCW	0.42	$0.42 \pm \text{n.d.}$	0.00	n.d.	n.d.	n.d.	66.86	71.12
+ GW (KHB)	0.43	$0.86 \pm 0.55$	0.43	n.d.	n.d.	$22.10 \pm 16.10$	71.05	87.36
+ MW (KHB)	0.55	$0.80 \pm 0.16$	0.73	$11.58 \pm 0.32$	304.15	$4.54 \pm 4.95$	64.88	145.62
+ MW (CB)	0.55	$0.92 \pm 0.18$	0.37	$10.93 \pm 0.30$	78.30	$10.80 \pm 7.83$	63.66	126.08
+ EW (CB)	0.45	$1.23 \pm 0.13$	0.78	$11.45 \pm 0.16$	346.66	$1.90 \pm 0.98$	64.28	124.70
+ $\text{FeCl}_3$	1.26	$1.37 \pm 0.27$	0.11	$11.37 \pm 0.51$	321.16	$17.10 \pm 19.70$	64.09	346.39

Dissolved iron concentration (dFe, measured via ICP-MS), total ligand concentration ( $L_T$ ), conditional stability constants ( $\log K_{\text{FeL,Fe}}^{\text{cond}}$ ), complexation capacity ( $\alpha = L_T \times 10^{\log K_{\text{FeL,Fe}}^{\text{cond}}}$ , where  $L_T$  is in  $\text{mol L}^{-1}$ ), concentration of free inorganic Fe ( $\text{Fe}'$ ). For  $L_T$ ,  $\log K_{\text{FeL,Fe}}^{\text{cond}}$ ,  $\alpha$  and  $\text{Fe}'$ , values are represented  $\pm$  the uncertainty of the fitting method. The natural Fe sources (subaerial groundwater seepage (GW), proglacial meltwater (MW), estuarine water (EW)) were sampled in King Haakon Bay (KHB) and Cumberland Bay (CB).

aggregates and highlights the importance of including abiotic controls in the experimental design to detect non-biological effects that retain  $^{55}\text{Fe}$  on the filter.

It has been shown that dissolved organic matter (DOM) can quickly (< 30 minutes) aggregate into polymer gels (transparent exopolymeric particles, TEP; 0.4–200  $\mu\text{m}^{50}$ ) and remain intact, even when filtered again<sup>51</sup>. Abiotic factors enhancing the aggregation potential in seawater include, amongst others, concentrations of multivalent cations by forming cross-linking bridges<sup>52</sup>. Since we lack a full assessment of cations in the HCW, we can only speculate that they contributed to aggregation. We are, however,

able to exclude that low pH fostered aggregation as the HCW was rather alkaline (pH 7.96)<sup>52</sup>. Two important factors in aggregation are the quantity and quality of DOM present in seawater<sup>52</sup>. Concentrations of dissolved organic carbon (DOC, as a proxy for DOM) at both sites (HCW:  $73.52 \pm 0.76 \mu\text{M}$ ; LCW:  $66.86 \pm 0.93 \mu\text{M}$ ), fall within the range measured in the SO<sup>53,54</sup>. Hence, the quality rather than quantity of DOM in the HCW appears to be the driving factor for aggregation in this case. The chemical composition of TEP precursors, primarily polysaccharides excreted by phytoplankton, differ depending on species composition and physiological status of the in situ phytoplankton community<sup>55,56</sup>. In particular, this

**Table 2 | Fe concentrations in ascorbic acid-treated, unfiltered samples from natural Fe sources**

	Fe (II) in unfiltered samples after ascorbic acid addition ( $\mu\text{M}$ )
GW (KHB)	10.17 $\pm$ 3.90
MW (KHB)	1.13 $\pm$ 0.06
MW (CB)	9.87 $\pm$ 1.37
EW (CB)	2.36 $\pm$ 0.40

Measurements were conducted using the ferrozine method after reduction of Fe(III) by ascorbic acid (15 min). The pool thus includes dissolved Fe(II), dissolved Fe(III) (if present) and easily reducible (amorphous) Fe oxides. Samples were measured on board the research vessel before the start of the experiment. Values represent the mean  $\pm$  SD ( $n = 3$ ). The corresponding dFe concentrations, as measured via ICP-MS, are presented in Supplementary Table 3.

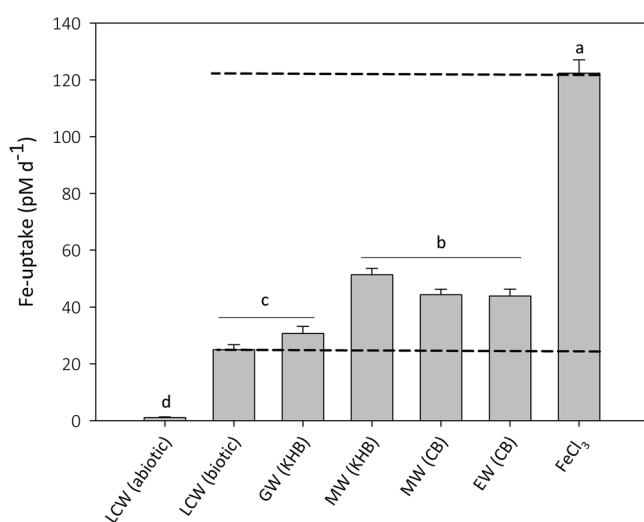


**Fig. 4 | Bioavailability of iron from nearshore sources from South Georgia.** For determination of Fe uptake, a diatom-dominated (Supplementary Fig. 1), pre-concentrated phytoplankton community was added to each treatment. Fe uptake rates of the phytoplankton community were measured in the low chlorophyll water (LCW), to which either natural unfiltered Fe sources (GW: groundwater from a subaerial seepage, MW: proglacial meltwater, EW: estuarine water) from King Haakon Bay (KHB) and Cumberland Bay (CB)) or  $\text{FeCl}_3$  were added. No additional Fe source was added to the LCW abiotic (without phytoplankton) and the LCW biotic (containing phytoplankton) treatment. Dashed lines indicate the lower and upper limit of Fe uptake. Statistically significant differences ( $p < 0.05$ ) are indicated by small letters. Values are displayed  $\pm$ SD,  $n = 3$ .

influences the tendency of DOM molecules to interact after collision (stickiness) and form gels/aggregates<sup>37</sup>. Several studies found that TEP formation is highest when phytoplankton are in exponential or senescent growth phases<sup>58–60</sup>. As described above, relative to the LCW, primary production of the HCW in situ phytoplankton community was five times higher, indicating an intense phytoplankton bloom at the time of sampling. In support of this, also the abundance of heterotrophic bacteria was 1.8 times higher in the HCW than in the LCW (Supplementary Table 1). Although the contribution of bacterially derived TEP precursors in the ocean appears to be negligible, it has been postulated that complex interactions of bacteria with phytoplankton can enhance the production of sticky TEP precursors (reviewed in ref. 61). Overall, the high biomass, productivity and bacterial abundance in the HCW were favorable for the release of sticky DOM, thus promoting the formation of <sup>55</sup>Fe-rich aggregates. Due to the latter, the biological Fe uptake processes of natural Fe sources in the HCW could not be quantified.

Bioavailability of Fe from different sources cannot be predicted from geochemical characteristics. Ground- and estuarine water and proglacial meltwaters were collected in KHB and CB. Fe concentrations of those unfiltered sources were determined on board the research vessel via the ferrozine method<sup>62</sup> (see methods section). Based on these values (Table 2), we calculated an enrichment of the LCW by 1 nM Fe from each source. Acknowledging the limitations of the ferrozine method, particles in the unfiltered sources can interfere with the photometric measurement, which might result in an overestimation of Fe concentrations. The dFe concentration in each of the LCW treatments was later determined in acidified samples via ICP-MS in the home laboratory (Table 1). Even though these concentrations were lower than expected, possibly due to overestimation of Fe concentrations in the source waters from the ferrozine measurements or Fe flocculation induced by salinity gradients, they were within a very narrow range, which is a prerequisite for comparing Fe uptake rates. We defined the Fe uptake rates in the “no addition” biotic LCW and the  $\text{FeCl}_3$  treatment as the lower and upper boundaries of bioavailability, respectively (Fig. 4). Accordingly, Fe from each source that significantly enhanced Fe uptake by phytoplankton compared to the biotic LCW was considered bioavailable. The range of Fe uptake was 97  $\text{pmol Fe L}^{-1} \text{d}^{-1}$  (lower boundary =  $25.05 \pm 0.25 \text{ pmol Fe L}^{-1} \text{d}^{-1}$ , upper boundary =  $122.38 \pm 4.69 \text{ pmol Fe L}^{-1} \text{d}^{-1}$ , Fig. 4). From the four natural sources, Fe from both MW’s and EW were bioavailable to the tested phytoplankton community, increasing Fe uptake by a factor of two compared to the biotic LCW (Fig. 4). The addition of GW, on the other hand, did not enhance Fe uptake compared to the biotic LCW suggesting that the Fe it contained was not, or only minimally, bioavailable. These widespread differences in Fe bioavailability of natural sources observed in the LCW were presumably caused by differences in Fe speciation. Yet, patterns of Fe speciation parameters corresponding to Fe uptake rates were not observed. In fact, the addition of natural Fe sources to the LCW considerably increased  $L_T$  by up to 193% (Table 1). However,  $L_T$  in the GW was twice as high compared to the LCW and similar to both MW’s, indicating no direct effect of ligands on the Fe bioavailability of the tested sources. Unexpectedly, the lowest  $L^*$  were found for MW (CB) and GW (0.37 and 0.43 nM, respectively).  $L_T$  was highest in the  $\text{FeCl}_3$  treatment, which is consistent with previous studies showing that ligands can be produced immediately when Fe is added to seawater<sup>63,64</sup>. Since  $\log K_{\text{FeL,Fe}'}^{\text{cond}}$  could not be determined for GW, evaluating if the binding strength of ligands in sources containing bioavailable vs. non-bioavailable Fe differs, is not possible. The variations in  $\log K_{\text{FeL,Fe}'}^{\text{cond}}$  and therefore also  $\alpha$  (78.30 to 346.66) for the three bioavailable Fe sources are, however, already large. Against expectations, Fe’ was highest in the GW and lowest in the EW, although the absence of a relationship between Fe’ and uptake rates might be explained by the uncertainty of calculating Fe’ in general. In line with our results, other studies that used Fe uptake rates to infer Fe bioavailability of a source also failed to identify trends in Fe speciation that could elucidate the underlying mechanisms governing bioavailability<sup>47,48,65</sup>. Also, ligand measurements were conducted under laboratory conditions with a fixed pH at room temperature, which does not resemble the conditions of our experiment. Therefore, the respective data should be interpreted with caution.

To assess whether the chemical composition of water from a source influences Fe bioavailability, we had a closer look at weathering processes. The bedrock geology at all our sampling sites is predominantly composed of andesitic volcanoclastic graywackes and shales<sup>66</sup>, indicating silicate weathering. Based on the measured dissolved ion concentrations in the GW and MW samples, calcium sulfate type-waters were identified (piper diagram, Supplementary Fig. 2). This result suggests pyrite oxidation and is supported by the high Fe concentrations, measured for these sources (Supplementary Table 3<sup>67</sup>). Pyrite oxidation is known to be microbially mediated and to increase silicate dissolution and promote Fe release<sup>68,69</sup>. Acid rock drainage, a result of pyrite oxidation<sup>38</sup> is a potential Fe source from land to the ocean. In

our study area, the GW (KHB) site exhibits reddish precipitates (Fig. 2), which can indicate acid rock drainage or dissimilatory Fe reduction<sup>70</sup>. The released Fe(II) is largely oxidized after being discharged. Previous studies conducted at the Antarctic peninsula proposed acid rock drainage as a putative bioavailable Fe source<sup>38</sup>. Based on our results, Fe deriving from GW (KHB) was not bioavailable to phytoplankton (Fig. 4). Thus an immediate Fe fertilization effect cannot be confirmed. This is in line with earlier findings, which described that diatom cultures were not able to access ferrihydrites as a Fe source, resulting in low uptake rates close to those of Fe bound to the strong siderophore desferrioxamine B<sup>23</sup>. However, freshly formed Fe oxides are important electron acceptors in early diagenesis and can potentially indirectly fuel primary production by releasing benthic Fe(II)<sup>71</sup>.

In our study, we investigated two meltwater Fe sources from the proglacial zone of land terminating glaciers. The geological setting of a glacier (weathering type and intensity, bedrock geology, and biogeochemical processes in the proglacial environment, such as exposure to oxygen) ultimately determines the concentration and speciation of Fe in meltwater<sup>72,73</sup>. MW (KHB) was turbid and milky, indicating that it was rich in suspended matter, i.e., glacial flour from the base of the glacier. Potentially it was sourced from an anoxic subglacial drainage system<sup>74</sup>, where microbial processes producing Fe(II) are typically enhanced<sup>75–77</sup>. MW (CB), on the other hand, was clear and its ionic strength (calcium, magnesium and silicon, Supplementary Table 3) was less than half compared to MW (KHB), suggesting that it was sourced from supraglacial melting, a highly oxidative environment. Unlike Fe(III), Fe(II) is dissolved, thus influencing the dFe inventory and bioavailability. Even though both meltwater streams were oxic, we expected differences in Fe bioavailability given the contrasting settings from which they originate. However, Fe from MW (KHB) and MW (CB) were equally bioavailable to phytoplankton. This suggests that geochemical processes in the proglacial environment determined Fe speciation and bioavailability, rather than the redox conditions at the melting locus of the glacier. Similar to our study, the Fe uptake rates were high in seawater samples collected in proximity to an Antarctic marine terminating glacier (Mertz Glacier), representing yet another geological setting<sup>47</sup>. Although up to 95% of the initial dFe in glacial meltwater can be lost due to scavenging processes<sup>72,78,79</sup> (precipitation or salinity gradient induced flocculation and particle adsorption in the proglacial and estuarine environment) a low flux of bioavailable Fe is supplied.

The EW was collected at the outlet of the proglacial meltwater stream, directly at the shoreline. As expected, uptake rates of Fe from the EW were similarly high to those of both MWs (Fig. 4), indicating elevated Fe bioavailability relative to the biotic LCW. This trend suggests the input of glacial meltwater into the EW, as also supported by its lower salinity (25.40, Supplementary Table 3). Furthermore, out of the four tested sources, EW was the only one, with a detectable level of humic substances (Supplementary Table 4), which in another laboratory study has been shown to enhance Fe uptake rates of phytoplankton<sup>36</sup>.

As expected, Fe in none of our natural sources approached the bioavailability of FeCl<sub>3</sub>. Interestingly, however, Fe in three of the four studied natural sources was similarly bioavailable to the same phytoplankton community, even though they originated from contrasting geochemical settings. This trend highlights that geochemical characterization (chemical and physical speciation and redox history) of Fe sources alone is not sufficient to predict Fe bioavailability and future studies need to link biological and geochemical approaches.

**Nearshore bioavailable Fe sources enhance offshore primary production.** The low Fe:C uptake ratio (4.23 μmol:mol) of the diatom-dominated phytoplankton community (Supplementary Fig. 1) indicates Fe limitation and thus depicts a realistic scenario of carbon fixation capacity for Antarctic offshore waters<sup>41,80–82</sup>. Consequently, MW (KHB), MW (CB), and EW, containing bioavailable Fe, would increase CO<sub>2</sub> fixation in open ocean waters (71 μg C L<sup>-1</sup> d<sup>-1</sup>) by 105, 77, and 75%, respectively (Table 1). We are currently observing an increase in global temperatures<sup>83</sup>, leading to altered Fe supply from melting glaciers and

thawing permafrost, with important biological and biogeochemical implications. The rise in temperatures on South Georgia will lead to thawing of the moraine and increase groundwater discharge, introducing copious amounts of Fe into the coastal environment. However, this study suggests that this source, with its limited Fe bioavailability, plays a minor role in fueling phytoplankton blooms off South Georgia. Meteorological records from South Georgia confirm a continuous warming trend since 1905 with increasing warm and dry westerly winds<sup>39</sup>. Modeling studies estimate that the maximum combined output of glacial discharge from South Georgia is  $1.0368 \times 10^8 \text{ m}^3 \text{ d}^{-1}$  in austral summer<sup>84,85</sup>. Using the dFe concentrations measured in MW (KHB) and MW (CB, Supplementary Table 3), the potential flux to the coastal ocean could range between  $7.4 \times 10^3$  and  $49.5 \times 10^3 \text{ mol dFe d}^{-1}$ . Long-term observations of South Georgia's glaciers show an overall retreat but heterogeneous regional patterns. With a mean elevation change of  $-1.76 \pm 0.01 \text{ m y}^{-1}$ , thinning rates were calculated to be highest for glaciers in the north east of the island and 2.5 times lower for glaciers in the south-west ( $-0.69 \pm 0.01 \text{ m y}^{-1}$ <sup>86</sup>). The warming-induced release of bioavailable Fe from glacial meltwaters from South Georgia into the surrounding waters could thus become an increasingly important Fe source in the future. In addition to glacial meltwater discharge in the mixing zone of the fjord, the EW is also influenced by other Fe sources, though their nature and origin are difficult to track. Fe originating from South Georgia's shelf was shown to fuel offshore phytoplankton blooms, based on modeling and observational studies<sup>13,14</sup>. Indeed, in this study, Fe from EW proved to be a bioavailable source to phytoplankton, with increasing proportions of glacial meltwater in the future.

Different to former studies, which assessed Fe bioavailability based solely on chemical characterization<sup>20,22,87</sup>, this study, quantified Fe bioavailability of nearshore sources via <sup>55</sup>Fe uptake rates of a natural phytoplankton community and linked the results to geochemical processes as well as the redox history of the Fe sources. This unique approach revealed that only glacial meltwaters, even when originating from different geological and redox settings, provide bioavailable Fe to phytoplankton, while groundwater did not. This finding was unexpected, since a previous geochemically based study claimed the bioavailability of Fe in groundwater transported into the coastal zone<sup>38</sup>. Our study also shows that the bioavailability of Fe from natural sources from South Georgia was primarily dependent on in situ biogeochemical interactions in seawater. Aggregates formed from DOM, likely resulting from microbial activity during a phytoplankton bloom, scavenged dFe and thereby made it unavailable to phytoplankton. This process was not observed for the low-biomass water, in which Fe released from MW and EW was bioavailable to phytoplankton. These results demonstrate the complexity and unpredictability of Fe bioavailability, which is dependent on the properties of the source itself and on the biogeochemical characteristics of the receiving water. Overall, this study reveals that Fe from glacial meltwater and water from the mixing zone of estuaries is bioavailable in low chl regions of the SO, fertilizing and enhancing CO<sub>2</sub> uptake by phytoplankton blooms.

## Methods

### Experimental design

During the GEOTRACES Process Study *Island Impact* (RV *Polarstern* expedition PS133/2, November and December 2022<sup>40</sup>), seawater was sampled at two stations in the Atlantic sector of the SO near South Georgia Island, first the station west of the island and second the station south of the island (Fig. 1). The two stations exhibited different chlorophyll biomass and are thus referred to as low chlorophyll water (LCW,  $0.33 \pm 0.01 \mu\text{g chl a L}^{-1}$ ) and high chlorophyll water (HCW,  $3.78 \pm 0.24 \mu\text{g chl a L}^{-1}$ ). Using a polyethylene hose connected to an ALMATEC teflon membrane pump, water from 20 m depth was pumped directly into a trace metal clean laboratory container and sampled under a laminar flow bench (US class 100, Opta, Bensheim, Germany). After flushing the hose for 45 minutes at each station, water for the experiment was filtered (0.2 μm) using a Sartorius Sartobran filter capsule, collected in carboys and stored at 2 °C in the dark

until the start of the experiment. All equipment used was trace metal cleaned according to GEOTRACES protocols<sup>88</sup>, and samples were processed using trace metal clean techniques. The Fe sources were collected from glacier outlet areas in King Haakon Bay (KHB) on the south-western side of the island and Cumberland Bay (CB) on the north-eastern side (Fig. 2 and Supplementary Table 3). A proglacial turbid meltwater (MW) stream and groundwater (GW) from a subaerial seepage with reddish precipitates was sampled in KHB. A clear proglacial meltwater stream and water from the estuary (EW) were sampled in CB. The EW was taken in the mixing zone, where the proglacial meltwater stream enters the fjord. All sampling sites were located approximately 1 km from the respective glacier terminus. For sampling, a Tygon tube connected to a peristaltic pump (Global Waters) was used, and bottles were rinsed three times with the sample before filling. In each source, Fe was measured as Fe(II), after addition of 50  $\mu$ l of ascorbic acid (1% w/v) to 1 mL of unfiltered sample. After 15 min, measurements were performed onboard according to ref. 89, using a DR Lange HACH 3900 photometer at the wavelength of 565 nm. The limit of detection for this method was 0.5  $\mu$ M. The resulting concentrations include Fe(II), Fe(III) and easily reducible amorphous Fe oxides, as these are dissolved by ascorbic acid. Particles could also have interfered with the photometric measurement. Comparison of data from the ferrozine analyses with dFe measurements of respective filtered samples (Table 2 and Supplementary Table 3) shows that only 1–6% of the concentrations determined by ferrozine derive from dFe, indicating a high amount of easily reducible amorphous Fe oxides in the natural Fe sources. Based on the ferrozine measurements (Table 2), an Fe enrichment of 1 nM through addition of each unfiltered Fe source was made to 0.2  $\mu$ m filtered LCW and HCW (Fig. 4). The volume of each Fe source water was less than 0.1% of the total incubation volume and dFe concentration in each treatment was analyzed in acidified and filtered samples via ICP-MS (Table 1; for detailed method description, see section dissolved Fe and major ion concentrations). The effect of the four natural Fe sources was also compared to the addition of 1 nM iron chloride (FeCl<sub>3</sub>), with the latter being considered highly bioavailable to phytoplankton<sup>90,91</sup>. In addition, a set of bottles containing the LCW and HCW were left unamended. All treatments (in triplicate) were left to equilibrate for 24 h at 2 °C in the dark. Subsequently, samples to determine the Fe speciation chemistry in each treatment were taken (0.2  $\mu$ m filtration).

### Dissolved Fe and major ion concentrations

About 100 mL of 0.2  $\mu$ m filtered sample water was acidified with double-distilled hydrochloric acid (HCl) to pH 1.7 and stored at 2 °C to determine dissolved Fe concentrations<sup>92</sup>. To avoid interferences with organic material, all samples were irradiated with UV light for 1.5 h, subsequently concentrated by a factor of 10, using a SeaFast system (Elemental Scientific, at the Alfred Wegener Institute), and spiked with a rhodium single-element standard. Dissolved Fe concentrations were then determined via inductively coupled plasma mass spectrometry (ICP-MS, Element2, Thermo Fisher Scientific). The instrument was tuned to achieve oxide formation rates below 0.3%. The accuracy of the analysis was verified by measuring certified reference material (NASS-7), which was diluted by a factor of 10 to match the expected low concentrations of Fe in the samples. With a recovery rate of 98% (certified value: 351  $\pm$  26 ng Fe L<sup>-1</sup>, measured value: 343.47  $\pm$  6.91 ng Fe L<sup>-1</sup>), the verification was found valid. For water chemistry analysis of the Fe sources (Piper Diagram), dissolved concentrations of Mg, Na, K, and Ca in the Fe sources were measured using Inductively Coupled Plasma Optical Emission Spectrometry (ICP-OES, Thermo Scientific iCAP 7000, at the Alfred Wegener Institute). To correct for variations in the ionic strength of the samples, an internal yttrium standard was used. The certified reference material for river water SLRS-6 revealed recovery rates of 94.93% ( $n$  = 6) for Ca, 88.12% ( $n$  = 6) for Mg, 106.31% ( $n$  = 2) for Na, 114.65% ( $n$  = 2) for K and 114.05% for Mg ( $n$  = 6). Sulfate (SO<sub>4</sub><sup>2-</sup>) and chloride (Cl<sup>-</sup>) anions were quantified using a Metrohm 930 Compact Ion Chromatography (IC) Flex system. Recoveries of a measured spiked IAPSO were 95.52% ( $n$  = 3) for SO<sub>4</sub><sup>2-</sup> and 95.71% ( $n$  = 3) for Cl<sup>-</sup>. To rule out the distortion of the Piper diagram by sea salt in our samples, we assessed the Na/Cl ratio and found

that it did not exceed 0.63. Thus, it remains well below the reference value of 0.86, indicating negligible sea salt contribution<sup>93</sup>.

### Fe speciation

About 500 mL of 0.2  $\mu$ m filtered water was frozen (–20 °C) for analysis of Fe speciation at the University of Washington. Competitive ligand exchange adsorptive cathodic stripping voltammetry<sup>94</sup> provided estimates for L<sub>T</sub> and associated conditional stability constants, using the artificial ligand salicylaldehyde (SA). A day before the analysis, samples were defrosted, and each one was aliquoted into 15 Teflon vials. Each aliquot was then buffered with boric acid to obtain a pH of 8.2 (NBS scale). Aliquots of the same sample were subsequently spiked with increasing concentrations of Fe, ranging from 0 to 25 nM to establish an equilibrium between the competing artificial ligand SA and the natural ligands. Following overnight equilibration, samples were analyzed on a BASi instrument using a controlled growth mercury (Hg) electrode. A standard Hg drop was used as a working electrode. A platinum wire counter electrode and a double-junction Ag/AgCl (3 M KCl) were used as counter- and reference electrodes. Peaks generated from the titrations were extracted using the ECDSOFT software package using a curved baseline, and the Fe-binding ligand parameters were derived by modeling using the ProMCC software<sup>95</sup>. The quantified parameters included ligand concentrations (L), conditional stability constants with respect to Fe<sup>2+</sup> ( $\log K_{\text{FeL,Fe}^{2+}}^{\text{cond}}$ ), and Fe<sup>2+</sup> concentrations. All ligand parameters were determined using the complete complexation fitting model in ProMCC, and were iterated until the root mean square error was minimized for all parameters. The total root mean square error, as expressed as a sum of all parameters in ProMCC, was less than 30 in all samples. To further resolve the natural ligand pool, the contribution of humic substances was measured at GEOMAR by means of catalytic cathodic stripping voltammetry, following ref. 96. The limit of detection for this method is 0.04 nM, HS concentrations were normalized using an iron-binding capacity of 14.6 nM Fe per 1 mg L<sup>-1</sup> of SRFA, allowing the expression of ligand concentrations in nM.

### Dissolved organic carbon (DOC)

About 500 mL of 0.2  $\mu$ m filtered water was frozen (–20 °C) and analyzed at GEOMAR for DOC using the high-temperature catalytic oxidation method, following<sup>97</sup>. Ultrapure (MilliQ) water was used to determine the instrument blank and was accepted for values <1  $\mu$ M C. Additionally, two internal standards with DOC concentrations matching those in the samples were prepared from potassium hydrogen phthalate (Merck 109017). Values for each sample are reported as the mean of four technical replicates  $\pm$  standard deviation.

### Macronutrient concentrations

About 20 mL of 0.2- $\mu$ m filtered water was frozen (–20 °C) to measure concentrations of nitrate, phosphate and silicate colorimetrically on a Seal AA500 Autoanalyzer at the Alfred Wegener Institute<sup>98</sup>.

### Fe-uptake assay

To measure intracellular Fe uptake and thereby assess bioavailability of Fe in each source, radioactive Fe (0.03 nM final concentration, <sup>55</sup>FeCl<sub>3</sub> = 9150 Bq; Perkin Elmer, MA, USA) was added to all treatments and left in the dark at 2 °C for 24 h, allowing the <sup>55</sup>Fe to equilibrate into the various Fe pools<sup>47,65,99</sup> (Fig. 3). Meanwhile, phytoplankton were gently concentrated (50x) from 40 L of seawater by gravity filtration (Millipore Amicon, model 8400) using a 3  $\mu$ m polycarbonate filter (Whatman Nucleopore, 90 mm), as described in ref. 41. Due to the fact that the phytoplankton concentrate led to clogging of the filter at the HCW site, we decided to collect a Fe-limited community from an offshore region (Fig. 1). A small aliquot (2 mL) of the concentrated phytoplankton community was then added to 2 L of each treatment to once again achieve ambient cell densities. From the 2 L bottle, three smaller incubation bottles of 100 mL were filled for each treatment. The LCW and HCW (without source additions) were further split into biotic and abiotic treatments, with and without the addition of phytoplankton concentrate,

respectively (Fig. 3). Since the same volume of phytoplankton concentrate was added to each biotic treatment, all contained the same biomass and species composition (Supplementary Fig. 1). An incubation period of 24 h was chosen to prevent shifts in species composition, which would have impeded the interpretation of  $^{55}\text{Fe}$  uptake rates between treatments. Within the incubation period of 24 h, primary production rates of the concentrated phytoplankton community were similar in the LCW and HCW ( $71.14 \pm 6.83 \text{ mg C m}^{-3} \text{ d}^{-1}$  and  $71.32 \pm 8.36 \text{ mg C m}^{-3} \text{ d}^{-1}$ , respectively), even though in situ biogeochemical characteristics of the LCW and HCW differed (e.g., aggregate formation). Each treatment was incubated at  $2^\circ\text{C}$  and  $30 \mu\text{mol photons m}^{-2} \text{ s}^{-1}$  light intensity (16:8 h light-dark cycle), resembling in situ conditions. After 24 h, cells were filtered onto  $2\text{-}\mu\text{m}$  polycarbonate filters, followed by three rinses with oxalate solution as well as three more rinses with  $0.2\text{-}\mu\text{m}$  filtered natural seawater. The oxalate wash was used to remove any loosely adsorbed Fe from the outside of the cells<sup>46</sup>. Counts per minute were determined on the shipboard liquid scintillation counter (Tri-Carb2900TR) after adding 5 mL scintillation cocktail (Ultima Gold, Perkin Elmer) to each filter. Using a custom quench curve and taking into account the radioactive decay, counts per minute were transformed to disintegrations per minute. Finally, intracellular Fe-uptake rates were calculated, using the total dFe concentration ( $\text{dFe}_{\text{total}} = \text{dFe}$  in each treatment (see Table 1) +  $^{55}\text{Fe}$  added) and incubation time (T), following<sup>48</sup>:

$$\text{Fe uptake} = ((^{55}\text{Fe}_{\text{filter}}/\text{TA}) * \text{dFe}_{\text{total}})/T \quad (1)$$

where  $^{55}\text{Fe}_{\text{filter}}$  is the activity on the filter and TA the total activity added. All incubations received the same volume of phytoplankton concentrate and were incubated for 24 h, assuming that biomass did not change. Therefore, Fe uptake rates were not additionally normalized to biomass.

### Chl a

To determine chl a concentration, 500 mL seawater was filtered onto glass-fiber filters (GF/F,  $0.7\text{-}\mu\text{m}$  pore size, Whatman, Wisconsin, USA) and stored at  $-20^\circ\text{C}$  until further analysis at the Alfred Wegener Institute. For extraction, filters were soaked in 90% acetone for 24 h at  $4^\circ\text{C}$  in the dark and subsequently analyzed on a Trilogy Fluorometer (Turner Design, San Jose, CA, USA), using the non-acidification module<sup>100</sup>.

### Taxonomic analysis

Quantification of heterotrophic bacteria in the in situ plankton communities at both sampling locations (LCW and HCW) was carried out by flow cytometry according to ref. 101. Briefly, unfiltered seawater was fixed with formalin (1% final concentration) and immediately frozen at  $-80^\circ\text{C}$  until analysis on a BD Accuri C6 Plus at the Alfred Wegener Institute. Rainbow fluorescent particles ( $2.1 \mu\text{m}$ , Spherotec) were added to each sample as a size and fluorescence reference. An abundance of heterotrophic bacteria was determined by staining the cells with SYBR green (Thermo Fischer). The effective removal of heterotrophic bacteria in the  $0.2 \mu\text{m}$  filtered LCW and HCW (i.e., water used for the experiment) was verified as the counts/mL were similar to those in samples containing MilliQ and SYBR green (difference of  $6 \pm 2\%$ ,  $n = 6$ ). Light microscopy was used for taxonomic identification (based on ref. 102) of the concentrated, diatom-dominated phytoplankton community (Supplementary Fig. 1), which was preserved in Lugol's solution (2% final concentration). According to the Utermöhl method<sup>103</sup>, a 10 mL aliquot was left to settle in a sedimentation chamber for 24 h before counting major taxa using an inverted microscope (Axiovert 200, Zeiss, at the Alfred Wegener Institute).

### Photosynthetic efficiency

Chl a fluorescence was assessed using a fast repetition rate fluorometer (FRRf, FastOcean PTX sensor, Chelsea Technologies Group Ltd., West Molesey, United Kingdom) in combination with a FastAct Laboratory system (Chelsea Technologies Group Ltd., West Molesey, United Kingdom). Measurements were performed at incubation temperature ( $2^\circ\text{C}$ ). Samples were dark acclimated for 45 min and subsequently exposed to 100

flashlets on a  $2\text{-}\mu\text{s}$  pitch (saturation of PSII in the single turnover mode), followed by a relaxation phase of 40 flashlets on a  $50\text{-}\mu\text{s}$  pitch. The maximum quantum yield of PSII ( $F_v/F_m$ ) was calculated from minimum ( $F_0$ ) and maximum ( $F_m$ ) chl a fluorescence:

$$F_v/F_m = (F_m - F_0)/F_m \quad (2)$$

### Primary production

Following the JGOFS protocol<sup>100</sup>, primary production of in situ communities at all three oceanic sampling sites (Fig. 1) was measured using  $^{14}\text{C}$ . Therefore, 50 mL of seawater was spiked with  $0.97 \text{ MBq}$  of  $^{14}\text{C}$  bicarbonate (Perkin Elmer, specific activity  $2035 \text{ MBq mmol}^{-1}$ ), incubated for 24 h at  $2^\circ\text{C}$  with a light intensity of  $30 \mu\text{mol photons m}^{-2} \text{ s}^{-1}$  and subsequently filtered onto a  $0.2 \mu\text{m}$  polycarbonate filter. The filter was then acidified with  $250 \mu\text{L}$   $1.2 \text{ N HCL}$  for 24 h, ensuring that any inorganic  $^{14}\text{C}$  left on the filter could degas. Total activity was determined in a  $250 \mu\text{L}$  aliquot of the incubation. Finally, 5 mL scintillation cocktail (Ultima Gold, Perkin Elmer) was added to the total activities, and the degassed filters and samples were counted on the shipboard scintillation counter (Tri-Carb2900TR).

### Statistical analysis

To test for statistically significant differences ( $p < 0.05$ ) of the different Fe sources within the HCW and LCW treatments, one-way analysis of variance (ANOVA), followed by Tukey's multiple comparison test were performed using the software GraphPad Prism (Version 10.2.2). Graphs were produced using the software Sigmaplot (Version 15.0) and Grapher (Version 20.2.321).

### Reporting summary

Further information on research design is available in the Nature Portfolio Reporting Summary linked to this article.

### Data availability

All data needed to evaluate the conclusions in the paper are present in the paper and/or the Supplementary Materials and are freely available from <https://doi.org/10.5281/zenodo.1752367>.

Received: 7 August 2025; Accepted: 2 December 2025;

Published online: 28 January 2026

### References

- de Baar, H. J. W. et al. Synthesis of iron fertilization experiments: from the iron age in the age of enlightenment. *J. Geophys. Res. I Oceans* **110**, 1–24 (2005).
- Martin, J. H. Glacial-interglacial  $\text{CO}_2$  change: the iron hypothesis. *Paleoceanography* **5**, 1–13 (1990).
- Basterretxea, G., Font-Muñoz, J. S., Hernández-Carrasco, I. & Sañudo-Wilhelmy, S. A. Global variability of high-nutrient low-chlorophyll regions using neural networks and wavelet coherence analysis. *Ocean Sci.* **19**, 973–990 (2023).
- Atkinson, A. et al. South Georgia, Antarctica: a productive, cold water, pelagic ecosystem. *Mar. Ecol. Prog. Ser.* **216**, 279–308 (2001).
- Blain, S. et al. A biogeochemical study of the island mass effect in the context of the iron hypothesis: Kerguelen Islands, Southern Ocean. *Deep Sea Res. I Oceanogr. Res. Pap.* **48**, 163–187 (2001).
- Doty, M. S. & Oguri, M. The island mass effect. *ICES J. Mar. Sci.* **22**, 33–37 (1956).
- Blain, S., Sarthou, G. & Laan, P. Distribution of dissolved iron during the natural iron-fertilization experiment KEOPS (Kerguelen Plateau, Southern Ocean). *Deep Sea Res II Top. Stud. Oceanogr.* **55**, 594–605 (2008).
- De Falco, C., Desbiolles, F., Bracco, A. & Pasquero, C. Island mass effect: a review of oceanic physical processes. *Front. Mar. Sci.* **9**, 894860 (2022).

9. Bowman, M. J., Dietrich, D. E. & Lin, C. A. in *Coastal and Estuarine Studies* (ed. Maul, G. A.) Ch. 2 (American Geophysical Union, 1996).
10. Hasegawa, D., Lewis, M. R. & Gangopadhyay, A. How islands cause phytoplankton to bloom in their wakes. *Geophys. Res. Lett.* **36**, L20605 (2009).
11. Schallenberg, C. et al. Sustained upwelling of subsurface iron supplies seasonally persistent phytoplankton blooms around the Southern Kerguelen Plateau, Southern Ocean. *J. Geophys. Res. Oceans* **123**, 5986–6003 (2018).
12. Arrigo, K. R., van Dijken, G. L. & Bushinsky, S. Primary production in the Southern Ocean, 1997–2006. *J. Geophys. Res. Oceans* **113**, C08004 (2008).
13. Schlosser, C. et al. Mechanisms of dissolved and labile particulate iron supply to shelf waters and phytoplankton blooms off South Georgia, Southern Ocean. *Biogeosciences* **15**, 4973–4993 (2018).
14. Borrione, I., Aumont, O., Nielsdóttir, M. C. & Schlitzer, R. Sedimentary and atmospheric sources of iron around South Georgia, Southern Ocean: a modelling perspective. *Biogeosciences* **11**, 1981–2001 (2014).
15. Nielsdóttir, M. C. et al. Seasonal and spatial dynamics of iron availability in the Scotia Sea. *Mar. Chem.* **130–131**, 62–72 (2012).
16. Monien, P. et al. Redox conditions and trace metal cycling in coastal sediments from the maritime Antarctic. *Geochim. Cosmochim. Acta* **141**, 26–44 (2014).
17. Tang, W. et al. Widespread phytoplankton blooms triggered by 2019–2020 Australian wildfires. *Nature* **597**, 370–375 (2021).
18. Nalivaev, A. et al. Glaciogenic iron transport pathways to the Kerguelen offshore phytoplankton bloom. Preprint at egusphere <https://doi.org/10.5194/egusphere-2025-2145> (2025).
19. Raiswell, R. et al. Iron in glacial systems: speciation, reactivity, freezing behavior, and alteration during transport. *Front. Earth Sci.* **6**, 2296–6463 (2018).
20. Bhatia, M. P. et al. Greenland meltwater as a significant and potentially bioavailable source of iron to the ocean. *Nat. Geosci.* **6**, 274–278 (2013).
21. Lancelot, C. et al. Spatial distribution of the iron supply to phytoplankton in the Southern Ocean: a model study. *Biogeosciences* **6**, 2861–2878 (2009).
22. Hopwood, M. J., Statham, P. J., Tranter, M. & Wadham, J. L. Glacial flours as a potential source of Fe(II) and Fe(III) to polar waters. *Biogeochemistry* **118**, 443–452 (2014).
23. Lis, H., Shaked, Y., Kranzler, C., Keren, N. & Morel, F. M. M. Iron bioavailability to phytoplankton: an empirical approach. *ISME J.* **9**, 1003–1013 (2015).
24. Bergquist, B. A., Wu, J. & Boyle, E. A. Variability in oceanic dissolved iron is dominated by the colloidal fraction. *Geochim. Cosmochim. Acta* **71**, 2960–2974 (2007).
25. Chen, M. & Wang, W. X. Bioavailability of natural colloid-bound iron to marine plankton: influences of colloidal size and aging. *Limnol. Oceanogr.* **46**, 1956–1967 (2001).
26. Chen, M., Dei, R. C. H., Wang, W. X. & Guo, L. Marine diatom uptake of iron bound with natural colloids of different origins. *Mar. Chem.* **81**, 177–189 (2003).
27. Mayer, L. M. Aggregation of colloidal iron during estuarine mixing: Kinetics, mechanism, and seasonality. *Geochim. Cosmochim. Acta* **46**, 2527–2535 (1982).
28. Borer, P. M., Sulzberger, B., Reichard, P. & Kraemer, S. M. Effect of siderophores on the light-induced dissolution of colloidal iron(III) (hydr)oxides. *Mar. Chem.* **93**, 179–193 (2005).
29. Dale, A. W. et al. A revised global estimate of dissolved iron fluxes from marine sediments. *Glob. Biogeochem. Cycles* **29**, 691–707 (2015).
30. Boyd, P. W. & Ellwood, M. J. The biogeochemical cycle of iron in the ocean. *Nat. Geosci.* **3**, 675–682 (2010).
31. Maldonado, M. T., Strzepek, R. F., Sander, S. & Boyd, P. W. Acquisition of iron bound to strong organic complexes, with different Fe binding groups and photochemical reactivities, by plankton communities in Fe-limited subantarctic waters. *Glob. Biogeochem. Cycles* **19**, 4 (2005).
32. Hassler, C. S. & Schoemann, V. Bioavailability of organically bound Fe to model phytoplankton of the Southern Ocean. *Biogeosciences* **6**, 2281–2296 (2009).
33. Hassler, C. et al. In *Oceanography and Marine Biology* (eds Gibson, R. N., Atkinson, R. J. A., Gordon, J. D. M. & Hughes, R. N.) 1–64 (CRC Press, 2012).
34. Shaked, Y. & Lis, H. Disassembling iron availability to phytoplankton. *Front. Microbiol.* **3**, 123 (2012).
35. Gledhill, M. & Buck, K. N. The organic complexation of iron in the marine environment: a review. *Front. Microbiol.* **3**, 69 (2012).
36. Hassler, C. S., Schoemann, V., Nichols, C. M., Butler, E. C. V. & Boyd, P. W. Saccharides enhance iron bioavailability to Southern Ocean phytoplankton. *Proc. Natl. Acad. Sci. USA* **108**, 1076–1081 (2011).
37. Hassler, C. S., Simó, R., Fawcett, S. E., Ellwood, M. J. & Jaccard, S. L. Marine biogenic humic substances control iron biogeochemistry across the Southern Ocean. *Nat. Commun.* **16**, 2662 (2025).
38. Dold, B. et al. Acid rock drainage and rock weathering in Antarctica: important sources for iron cycling in the Southern Ocean. *Environ. Sci. Technol.* **47**, 6129–6136 (2013).
39. Thomas, Z. et al. A new daily observational record from Grytviken, South Georgia: exploring twentieth-century extremes in the South Atlantic. *J. Clim.* **31**, 1743–1755 (2018).
40. Kasten, S. The Expedition PS133/2 of the research vessel POLARSTERN to the Scotia Sea in 2022. [https://doi.org/10.57738/BzPM\\_0775\\_2023](https://doi.org/10.57738/BzPM_0775_2023) (2023).
41. Trimbom, S., Hoppe, C. J. M., Taylor, B. B., Bracher, A. & Hassler, C. Physiological characteristics of open ocean and coastal phytoplankton communities of Western Antarctic Peninsula and Drake Passage waters. *Deep Sea Res. I Oceanogr. Res. Pap.* **98**, 115–124 (2015).
42. Marchetti, A. et al. Ferritin is used for iron storage in bloom-forming marine pennate diatoms. *Nature* **457**, 467–470 (2009).
43. Twining, B. S. & Baines, S. B. The trace metal composition of marine phytoplankton. *Ann. Rev. Mar. Sci.* **5**, 191–215 (2013).
44. Boyd, P. W. & Tagliabue, A. Using the L\* concept to explore controls on the relationship between paired ligand and dissolved iron concentrations in the ocean. *Mar. Chem.* **173**, 52–66 (2015).
45. Hunter, K. A. & Boyd, P. W. Iron-binding ligands and their role in the ocean biogeochemistry of iron. *Environ. Chem.* **4**, 221–232 (2007).
46. Hassler, C. S. et al. Iron associated with exopolymeric substances is highly bioavailable to oceanic phytoplankton. *Mar. Chem.* **173**, 136–147 (2015).
47. Fourquez, M. et al. Chasing iron bioavailability in the Southern Ocean: Insights from *Phaeocystis antarctica* and iron speciation. *Sci. Adv.* **9**, eadf9696 (2023).
48. Böckmann, S. et al. Salp fecal pellets release more bioavailable iron to Southern Ocean phytoplankton than krill fecal pellets. *Curr. Biol.* **31**, 2737–2746.e3 (2021).
49. Cabanes, D. J. E. et al. Using Fe chemistry to predict Fe uptake rates for natural plankton assemblages from the Southern Ocean. *Mar. Chem.* **225**, 103853 (2020).
50. Passow, U. Formation of transparent exopolymer particles, TEP, from dissolved precursor material. *Mar. Ecol. Prog. Ser.* **192**, 1–11 (2000).
51. Chin, W.-C., Orellana, M. V. & Verdugo, P. Spontaneous assembly of marine dissolved organic matter into polymer gels. *Nature* **391**, 568–572 (1998).
52. He, W., Chen, M., Schlautman, M. A. & Hur, J. Dynamic exchanges between DOM and POM pools in coastal and inland aquatic ecosystems: A review. *Sci. Total Environ.* **552**, 415–428 (2016).

53. Hansell, D. A., Carlson, C. A., Repeta, D. J. & Schlitzer, R. Dissolved organic matter in the ocean - a controversy stimulates new insights. *Oceanography* **22**, 202–211 (2009).
54. Lovecchio, E. et al. Export of Dissolved Organic Carbon (DOC) compared to the particulate and active fluxes near South Georgia, Southern Ocean. *Deep Sea Res. II Top. Stud. Oceanogr.* **212**, 105338 (2023).
55. Myklestad, S. M. Release of extracellular products by phytoplankton with special emphasis on polysaccharides. *Sci. Total Environ.* **165**, 155–164 (1995).
56. Aluwihare, L. & Repeta, D. A comparison of the chemical characteristics of oceanic DOM and extracellular DOM produced by marine algae. *Mar. Ecol. Prog. Ser.* **186**, 105–117 (1999).
57. Mopper, K. et al. The role of surface-active carbohydrates in the flocculation of a diatom bloom in a mesocosm. *Deep Sea Res. II Top. Stud. Oceanogr.* **42**, 47–73 (1995).
58. Mari, X. & Burd, A. Seasonal size spectra of transparent exopolymeric particles (TEP) in a coastal sea and comparison with those predicted using coagulation theory. *Mar. Ecol. Prog. Ser.* **171**, 63–76 (1998).
59. Passow, U. et al. The origin of transparent exopolymer particles (TEP) and their role in the sedimentation of particulate matter. *Cont. Shelf Res.* **21**, 327–346 (2001).
60. Engel, A. The role of transparent exopolymer particles (TEP) in the increase in apparent particle stickiness ( $\alpha$ ) during the decline of a diatom bloom. *J. Plankton Res.* **22**, 485–497 (2000).
61. Passow, U. Transparent exopolymer particles (TEP) in aquatic environments. *Prog. Oceanogr.* **55**, 287–333 (2002).
62. Köster, M. et al. Evolution of (bio-)geochemical processes and diagenetic alteration of sediments along the Tectonic migration of ocean floor in the Shikoku Basin off Japan. *Geochem. Geophys. Geosyst.* **22**, e2020GC009585 (2021).
63. Sijerčić, A. & Price, N. Hydroxamate siderophore secretion by *Pseudoalteromonas haloplanktis* during steady-state and transient growth under iron limitation. *Mar. Ecol. Prog. Ser.* **531**, 105–120 (2015).
64. Buck, K. N., Selph, K. E. & Barbeau, K. A. Iron-binding ligand production and copper speciation in an incubation experiment of Antarctic Peninsula shelf waters from the Bransfield Strait, Southern Ocean. *Mar. Chem.* **122**, 148–159 (2010).
65. Shaked, Y., Buck, K. N., Mellett, T. & Maldonado, M. T. Insights into the bioavailability of oceanic dissolved Fe from phytoplankton uptake kinetics. *ISME J.* **14**, 1182–1193 (2020).
66. Curtis, M. L. *Geological Map of South Georgia*. (2001).
67. Langmuir, D. *Aqueous Environmental Geochemistry* (Prentice-Hall, 1997).
68. Raiswell, R., Benning, L. G., Davidson, L., Tranter, M. & Tulaczyk, S. Schwertmannite in wet, acid, and oxic microenvironments beneath polar and polythermal glaciers. *Geology* **37**, 431–434 (2009).
69. Wadham, J. L. et al. Biogeochemical weathering under ice: Size matters. *Glob. Biogeochem. Cycles* **24**, GB3025 (2010).
70. Henkel, S., Kasten, S., Hartmann, J. F., Silva-Busso, A. & Staubwasser, M. Iron cycling and stable Fe isotope fractionation in Antarctic shelf sediments, King George Island. *Geochim. Cosmochim. Acta* **237**, 320–338 (2018).
71. Henkel, S., Kasten, S., Poulton, S. W. & Staubwasser, M. Determination of the stable iron isotopic composition of sequentially leached iron phases in marine sediments. *Chem. Geol.* **421**, 93–102 (2016).
72. Zhang, R. et al. Transport and reaction of iron and iron stable isotopes in glacial meltwaters on Svalbard near Kongsfjorden: From rivers to estuary to ocean. *Earth Planet Sci. Lett.* **424**, 201–211 (2015).
73. Tranter, M. & Wadham, J. L. In *Treatise on Geochemistry: Second Edition* (Elsevier Inc., 2013).
74. Hindshaw, R. S., Heaton, T. H. E., Boyd, E. S., Lindsay, M. R. & Tipper, E. T. Influence of glaciation on mechanisms of mineral weathering in two high Arctic catchments. *Chem. Geol.* **420**, 37–50 (2016).
75. Henkel, S. et al. Stable iron isotope signals indicate a “pseudo-abiotic” process driving deep iron release in methanic sediments. *Biogeosciences* **22**, 1673–1696 (2025).
76. Schnakenberg, A. et al. Electron acceptor availability shapes anaerobically methane oxidizing Archaea (ANME) Communities in South Georgia sediments. *Front. Microbiol.* **12**, 617280 (2021).
77. Wunder, L. C. et al. Iron and sulfate reduction structure microbial communities in (sub-)Antarctic sediments. *ISME J.* **15**, 3587–3604 (2021).
78. Sholkovitz, E. R. The flocculation of dissolved Fe, Mn, Al, Cu, Ni, Co and Cd during estuarine mixing. *Earth Planet Sci. Lett.* **41**, 77–86 (1978).
79. Schroth, A. W., Crusius, J., Hoyer, I. & Campbell, R. Estuarine removal of glacial iron and implications for iron fluxes to the ocean. *Geophys. Res. Lett.* **41**, 3951–3958 (2014).
80. Twining, B. S., Baines, S. B. & Fisher, N. S. Element stoichiometries of individual plankton cells collected during the Southern Ocean Iron Experiment (SOFeX). *Limnol. Oceanogr.* **49**, 2115–2128 (2004).
81. Strzepek, R. F., Maldonado, M. T., Hunter, K. A., Frew, R. D. & Boyd, P. W. Adaptive strategies by Southern Ocean phytoplankton to lessen iron limitation: uptake of organically complexed iron and reduced cellular iron requirements. *Limnol. Oceanogr.* **56**, 1983–2002 (2011).
82. Balaguer, J. et al. Iron and manganese availability drives primary production and carbon export in the Weddell Sea. *Curr. Biol.* **33**, 4405–4414 (2023).
83. Calvin, K. et al. *IPCC, 2023: Climate Change 2023: Synthesis Report. Contribution of Working Groups I, II and III to the Sixth Assessment Report of the Intergovernmental Panel on Climate Change* (eds Core Writing Team, H. Lee, H. & Romero, J.) (IPCC, 2023)
84. Matano, R. P., Combes, V., Young, E. F. & Meredith, M. P. Modeling the impact of ocean circulation on chlorophyll blooms around South Georgia, Southern Ocean. *J. Geophys. Res. Oceans* **125**, e2020JC01639 (2020).
85. Young, E. F., Meredith, M. P., Murphy, E. J. & Carvalho, G. R. High-resolution modelling of the shelf and open ocean adjacent to South Georgia, Southern Ocean. *Deep Sea Res. II Top. Stud. Oceanogr.* **58**, 1540–1552 (2011).
86. Fariás-Barahona, D. et al. Detailed quantification of glacier elevation and mass changes in South Georgia. *Environ. Res. Lett.* **15**, 034036 (2020).
87. Raiswell, R., Benning, L. G., Tranter, M. & Tulaczyk, S. Bioavailable iron in the Southern Ocean: the significance of the iceberg conveyor belt. *Geochem. Trans.* **9**, 7 (2008).
88. Cutter, G. et al. *Sampling and Sample-Handling Protocols for GEOTRACES Cruises*. <http://www.geotraces.org/sic/intercalibrate-data/cookbook> (2017).
89. Stookey, L. L. Ferrozine—a new spectrophotometric reagent for iron. *Anal. Chem.* **42**, 779–781 (1970).
90. Shaked, Y., Kustka, A. B. & Morel, F. M. M. A general kinetic model for iron acquisition by eukaryotic phytoplankton. *Limnol. Oceanogr.* **50**, 872–882 (2005).
91. Morel, F. M. M., Kustka, A. B. & Shaked, Y. The role of unchelated Fe in the iron nutrition of phytoplankton. *Limnol. Oceanogr.* **53**, 400–404 (2008).
92. Middag, R. et al. Intercomparison of dissolved trace elements at the Bermuda Atlantic Time Series station. *Mar. Chem.* **177**, 476–489 (2015).
93. Möller, D. The Na/Cl ratio in rainwater and the sea salt chloride cycle. *Tellus B* **42**, 254–262 (1990).

94. Moore, L. E., Heller, M. I., Barbeau, K. A., Moffett, J. W. & Bundy, R. M. Organic complexation of iron by strong ligands and siderophores in the eastern tropical North Pacific oxygen deficient zone. *Mar. Chem.* **236**, 104021 (2021).
95. Omanović, D., Garnier, C. & Pižeta, I. ProMCC: an all-in-one tool for trace metal complexation studies. *Mar. Chem.* **173**, 25–39 (2015).
96. Sukekava, C., Downes, J., Slagter, H. A., Gerringa, L. J. A. & Laglera, L. M. Determination of the contribution of humic substances to iron complexation in seawater by catalytic cathodic stripping voltammetry. *Talanta* **189**, 359–364 (2018).
97. Sugimura, Y. & Suzuki, Y. A high-temperature catalytic oxidation method for the determination of non-volatile dissolved organic carbon in seawater by direct injection of a liquid sample. *Mar. Chem.* **24**, 105–131 (1988).
98. Grasshoff, K., Kremling, K. & Ehrhardt, M. (eds) *Methods of Seawater Analysis* (Wiley, 1999).
99. Hassler, C. S., Alasonati, E., Mancuso Nichols, C. A. & Slaveykova, V. I. Exopolysaccharides produced by bacteria isolated from the pelagic Southern Ocean - role in Fe binding, chemical reactivity, and bioavailability. *Mar. Chem.* **123**, 88–98 (2011).
100. Intergovernmental Oceanographic Commission. *Protocols for the Joint Global Ocean Flux Study (JGOFS) Core Measurement* (UNESCO, 1994).
101. Koch, F. et al. The effect of vitamin B<sub>12</sub> on phytoplankton growth and community structure in the Gulf of Alaska. *Limnol. Oceanogr.* **56**, 1023–1034 (2011).
102. Scott, F. J. & Marchant, H. J. (eds) *Antarctic Marine Protists* (Australian Biological Resources Study/Australian Antarctic Division, 2005).
103. Utermöhl, H. Zur Vervollkommnung der quantitativen Phytoplankton-Methodik. *SIL Commun.* **9**, 1–38 (1958).
104. Dorschel, B. et al. The International Bathymetric chart of the Southern Ocean Version 2. *Sci. Data* **9**, 275 (2022).

## Acknowledgements

We thank Joshua Hübner for assistance during the experiment, Male Köster (Alfred Wegener Institute) for the onboard ferrozine measurements, Kai-Uwe Ludwichowski (Alfred Wegener Institute) for measuring macronutrient concentrations and Grit Steinhöfel-Sasgen (Alfred Wegener Institute) for valuable advice and insights on weathering processes. Further, we thank the captain and crew of RV Polarstern crew for their support during the expedition. This study was funded by the Alfred Wegener Institute (Grants No. AWI\_PS133/2\_04 and AWI\_PS133/2\_05). J.S. and B.E. were funded by the International Science Program for Integrative Research in Earth Systems (INSPIRES) at the Alfred Wegener Institute as part of the current research program in PoF IV. The *Island Impact* expedition was conducted under the GEOTRACES program as a process study. I acknowledge support by the Open Access publication fund of Alfred-Wegener-Institut Helmholtz-Zentrum für Polar- und Meeresforschung.

## Author contributions

Conceptualization of the study by F.K. and S.T. Samples were collected by J.S., F.K. and B.E. Sample analysis was performed by J.S., F.K., B.E., C.V., C.F.S., and A.R. The original draft was written by J.S. and reviewed and edited by J.S., F.K., B.E., C.V., R.Z., C.F.S., S.G.S., S.H., R.M.B., A.R., S.K., and S.T.

## Funding

Open Access funding enabled and organized by Projekt DEAL.

## Competing interests

The authors declare no competing interests.

## Additional information

**Supplementary information** The online version contains supplementary material available at <https://doi.org/10.1038/s43247-025-03092-5>.

**Correspondence** and requests for materials should be addressed to Jasmin Stimpfle.

**Peer review information** *Communications Earth and Environment* thanks the anonymous reviewers for their contribution to the peer review of this work. Primary Handling Editors: José Luis Iriarte Machuca and Alice Drinkwater. A peer review file is available.

**Reprints and permissions information** is available at <http://www.nature.com/reprints>

**Publisher's note** Springer Nature remains neutral with regard to jurisdictional claims in published maps and institutional affiliations.

**Open Access** This article is licensed under a Creative Commons Attribution 4.0 International License, which permits use, sharing, adaptation, distribution and reproduction in any medium or format, as long as you give appropriate credit to the original author(s) and the source, provide a link to the Creative Commons licence, and indicate if changes were made. The images or other third party material in this article are included in the article's Creative Commons licence, unless indicated otherwise in a credit line to the material. If material is not included in the article's Creative Commons licence and your intended use is not permitted by statutory regulation or exceeds the permitted use, you will need to obtain permission directly from the copyright holder. To view a copy of this licence, visit <http://creativecommons.org/licenses/by/4.0/>.

© The Author(s) 2025